analytical chemistry

pubs.acs.org/ac

Article

AIE Fluorescent Nanozyme-Enabled Ratiometric Sensing Platform for Selective Detection of Ascorbic Acid and Alkaline Phosphatase

Xiaoyu Wang,* Sijie Li, Si Zhang, Qi Sun, Qing Cheng, Ke Bao, Bing Xia, and Hui Wei*

Cite This: https://doi.org/10.1021/acs.analchem.5c07377

Read Online

ACCESS | Metrics & More | Article Recommendations | Supporting Information

ABSTRACT: Ascorbic acid (AA) and alkaline phosphatase (ALP) are essential biomolecules involved in numerous physiological and pathological processes. However, conventional nanozyme assays based on AA reduction or ALP-mediated AA generation often suffer from interference from coexisting reductants, compromising their selectivity and analytical reliability. Here, we reported a rationally designed fluorescent nanozyme, ZIF-8/Ru@TPE, constructed by anchoring ultrasmall Ru nanoparticles onto ZIF-8 and assembling them with the aggregation-induced emission (AIE) luminogen tetraphenylethylene (TPE). The resulting hybrid exhibited strong intrinsic fluorescence at 445 nm and remarkable peroxidase-like activity. Upon the addition of H_2O_2 and *o*-phenylenediamine (OPD), ZIF-8/Ru@TPE catalyzed OPD oxidation to form the fluorescent product 2,3-diaminophenazine (DAP), yielding a distinct emission peak at 570 nm while quenching the TPE fluorescence at 445 nm. Notably, AA triggered a self-amplified ratiometric response by simultaneously inhibiting OPD oxidation and generating an additional fluorophore through the reaction of dehydroascorbic acid with OPD, achieving high selectivity over other reductants. Exploiting ALP-catalyzed AA production, this platform was successfully extended to ALP activity determination in serum. This study presents a versatile nanozyme-based ratiometric sensing strategy for selective detection of AA and ALP, offering great potential for accurate bioanalysis in complex samples.

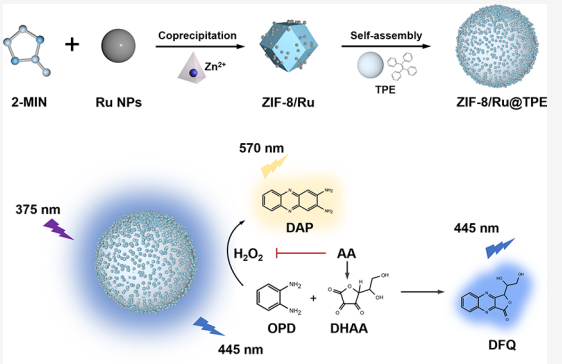

INTRODUCTION

Nanozymes, nanomaterials with enzyme-like catalytic activities that follow enzyme kinetics under physiological conditions, have emerged as robust and cost-effective alternatives to natural enzymes.[1−4] Nanozymes possess distinct advantages arising from their nanoscale features, including large surface areas for bioconjugation, tunable catalytical activities, and multifunctionalities beyond catalysis.[2,5−10] By coupling their catalytic behavior with unique physiochemical properties, nanozymes have been extensively applied in both *in vitro* sensing and *in vivo* bioanalysis for diverse targets detection, ranging from metal ions and small molecules to macromolecules, exosomes, and cells.[11−26] Despite these advances, limited selectivity compromises the reliability of nanozyme-enabled analytical methods.[27−29] Nanozyme selectivity can be improved through active-site engineering, molecular imprinting, or constructing enzyme-like substrate channels to regulate molecular access and tailor local microenvironments;[27−32] alternatively, assay selectivity can be introduced via external attributes, such as coupling with oxidases or functionalizing nanozymes with affinity ligands (e.g., antibodies and aptamers).[33−35] Nevertheless, selectively detecting reducing substances remains challenging because they are typically quantified by modulating nanozyme activity or reducing oxidized products, yielding similar responses from competing reductants.

Among various reducing substances, ascorbic acid (AA) plays a vital role in maintaining redox homeostasis, neuroprotection, and cellular defense.[36] Because it cannot be synthesized endogenously, AA must be acquired through diet or supplementation, making its accurate quantification particularly important. Previous AA assays typically exploited its strong reducing ability to quench nanozyme-catalyzed oxidation products (e.g., oxidized TMB), producing turn-off colorimetric or fluorescent signals.[37−40] However, these reduction-based strategies often suffered from poor selectivity, as other reductants such as glutathione (GSH) and cysteine produced similar responses.[37,41,42] As a result, most of these approaches measured total antioxidant capacity (TAC) rather than specifically quantifying AA.[37,41,43,44] In addition, alkaline phosphatase (ALP), a widely distributed hydrolase, is an

Received: November 25, 2025
Revised: January 19, 2026
Accepted: February 3, 2026

important biomarker for liver dysfunction, bone disorders, and biliary obstruction.[45,46] ALP assays relied on hydrolysis of phosphate esters such as ascorbic acid 2-phosphate to generate AA, which subsequently reduced oxidized products to produce measurable signals.[38,47,48] During ALP assays in complex biological matrices, coexisting reductants may lead to signal interference. These limitations highlight the need for innovative sensing strategies that enable highly selective detection of AA or ALP.

On the other hand, despite substantial progress in nanozyme-based sensing, most existing platforms—including those for AA or ALP detection—still relied on single-signal outputs, making them susceptible to environmental fluctuations and instrumental variation. In contrast, ratiometric fluorescence sensing offered enhanced analytical reliability by minimizing nonspecific interference through the use of the ratio between two emission signals.[40,49−52] In many nanozyme systems, the responsive signal originated from nanozyme-catalyzed oxidation of *o*-phenylenediamine (OPD) into the fluorescent product (i.e., 2,3-diaminophenazine, DAP).[12,49] However, constructing a reliable nanozyme-based ratiometric platform required an additional fluorescence channel with well-matched excitation and emission characteristics.

To address these challenges, we rationally designed a dual-functional fluorescent nanozyme, ZIF-8/Ru@TPE, by anchoring ultrasmall Ru nanoparticles onto ZIF-8 and subsequently assembling them with the aggregation-induced emission (AIE) luminogen tetraphenylethylene (TPE). This hybrid integrated intrinsic fluorescence and peroxidase-like activity, enabling the construction of a ratiometric fluorescence sensing platform. Upon exposure to H_2O_2 and OPD, ZIF-8/Ru@TPE catalyzed OPD oxidation to form fluorescent DAP, yielding a reaction-induced emission at 570 nm while partially quenching the TPE fluorescence at 445 nm. The emission ratio (F_{570}/F_{445}) was employed for reliable quantification of H_2O_2 and glucose, demonstrating a wider linear range and lower detection limits than single-signal assays. Notably, AA induced a self-amplified ratiometric response by simultaneously inhibiting OPD oxidation and forming an additional fluorophore, 3-(1,2-dihydroxyethyl)furo[3,4-*b*]quinoxalin-1(3H)-one (DFQ), through its oxidation product dehydroascorbic acid (DHAA) reacting with OPD, affording exceptional selectivity over other reductants. Furthermore, by exploiting ALP-catalyzed hydrolysis of phosphate esters to generate AA, the sensing platform was successfully extended to ALP activity determination. The practical applicability was validated by accurate quantification of AA in vitamin tablets and beverages, as well as ALP activity measurement in serum with satisfactory recoveries. Collectively, this study presents a versatile nanozyme-based ratiometric sensing strategy that integrates catalytic and fluorescent functionalities within a single nanostructure, offering a powerful platform for bioanalysis in complex matrices.

EXPERIMENTAL SECTION

Chemicals and Materials

Zinc nitrate hexahydrate ($Zn(NO_3)_2{\cdot}6H_2O$), ruthenium chloride ($RuCl_3$), tetrahydrofuran, *o*-phenylenediamine (OPD), glucose, glucose oxidase (GOx), ascorbic acid (AA), L-ascorbic acid 2-phosphate trisodium salt (AAP) were purchased from Aladdin Chemical Co., Ltd. Polyvinylpyrrolidone (PVP, M_w 55000) and alkaline phosphatase (ALP) were obtained from Sigma-Aldrich. Fetal bovine serum was purchased from Zhejiang Tianhang Biotechnology Co., Ltd. Ethylene glycol, acetone, nitric acid (HNO_3), and hydrogen peroxide (H_2O_2, 30%) were purchased from Sinopharm Chemical Reagent Co., Ltd. Methanol was purchased from Wuxi Yasheng Chemical Co., Ltd. Hydrochloric acid (HCl) was purchased from Nanjing Chemical Reagent Co., Ltd. Tetraphenylethylene (TPE) and 2-methylimidazole were obtained from J&K Scientific Co., Ltd. All aqueous solutions used in the experiments were prepared with deionized water (18.2 MΩ·cm, Millipore).

Instrumentation

Transmission electron microscopy (TEM) imaging was performed on a Tecnai 12 (Philips company, Holland) transmission electron microscope at an acceleration voltage of 120 kV. High-resolution transmission electron microscopy (HRTEM), high-angle annular dark-field scanning TEM (HAADF-STEM), and the corresponding energy-dispersive spectroscopy (EDS) elemental mappings were performed on an FEI Tecnai G2 F30 S-Twin TEM equipped with an acceleration voltage of 300 kV and an EDS detector, respectively. Scanning electron microscopy (SEM) imaging was performed on an FEI Inspect F50 or a ZEISS Merlin Compact scanning electron microscope. Powder X-ray diffraction (XRD) patterns were measured by a Bruker D8 advance diffractometer at 5°/min using a Cu Kα radiation. Hydrodynamic size and zeta potentials were measured on a Nano sizer ZS90 (Malvern Instruments, UK). Absorption spectra were collected using a UV-2700 spectrophotometer (Shimadzu, Japan). Fluorescence spectra were recorded using an FS5 fluorescence spectrometer (Edinburgh Instruments, UK). The fluorescence of the 96-well plate at 445 and 570 nm was recorded by a BioTek Cytation 3 microplate reader (Agilent, USA). X-ray photoelectron spectra (XPS) were obtained by using a Thermo Scientific Nexsa G2 surface analysis system. Inductively coupled plasma-optical emission spectroscopy (ICP-OES) measurements were conducted using a Thermo Scientific iCAP PRO spectrometer.

Synthesis of Ru, ZIF-8/Ru, and ZIF-8/Ru@TPE

Ru nanoparticles were synthesized following a previously reported procedure.[24] Briefly, 20.7 mg of $RuCl_3$, 100 mg of polyvinylpyrrolidone (PVP, M_w 55000), and 10 mL of ethylene glycol were mixed in a flask and heated to 120 °C under continuous stirring for 20 min. The temperature was then increased to 195 °C and maintained for 1 h. After cooling to room temperature, the resulting product was washed three times with acetone and subsequently redispersed in 5 mL of methanol via ultrasonication.

The ZIF-8/Ru was synthesized as follows. $Zn(NO_3)_2{\cdot}6H_2O$ (0.595 g) was dissolved in 20 mL of methanol, while 2-methylimidazole (0.657 g) was added to another 20 mL of methanol containing 6.65 mg of Ru. The two solutions were then mixed and stirred at room temperature for 4 h. After the reaction, the resulting product was collected by centrifugation (11000 rpm, 5 min), washed three times with methanol, and subsequently dried under vacuum at 40 °C overnight.

The ZIF-8/Ru@TPE was synthesized as follows. ZIF-8/Ru (40 mg) was dispersed in 20 mL of deionized water, while TPE (20 mg) was dissolved in 1 mL of tetrahydrofuran (THF). The two solutions were then mixed and stirred at room temperature in the dark for 2 h. After the reaction, the resulting product was collected by centrifugation (13000 rpm, 5 min), washed three times with deionized water, and subsequently dried under vacuum at 40 °C overnight.

The synthesis of ZIF-8 was carried out using the same procedure as that for ZIF-8/Ru, except that no Ru nanoparticles were introduced during the synthesis. Likewise, ZIF-8@TPE was prepared following the same protocol as ZIF-8/Ru@TPE, with ZIF-8 substituted for ZIF-8/Ru in the self-assembly process.

Peroxidase-like Activity Measurements

The peroxidase-like activities of ZIF-8/Ru and ZIF-8/Ru@TPE were evaluated using steady-state kinetics assays.[53,54] Briefly, the assays were performed at 26 °C in a 96-well microplate with H_2O_2 and TMB as substrates, and the absorbance changes were recorded using a microplate reader. A 0.2 M acetate buffer (pH 4.5) was employed as

https://doi.org/10.1021/acs.analchem.5c07377
Anal. Chem. XXXX, XXX, XXX−XXX

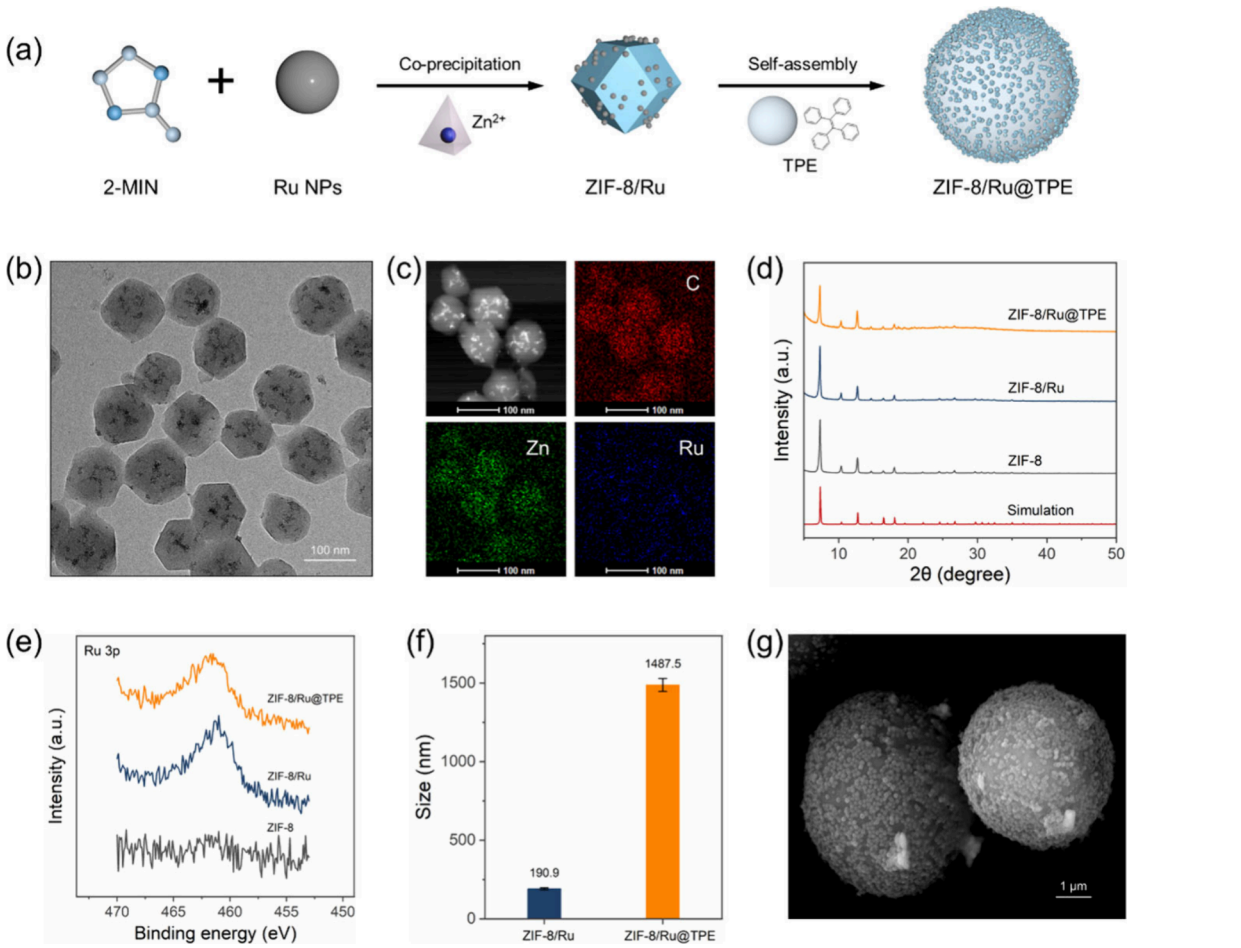

Figure 1. (a) Schematic illustration of the synthetic route of ZIF-8/Ru@TPE. (b) TEM image of ZIF-8/Ru. (c) HAADF-STEM image and corresponding EDS elemental mapping of ZIF-8/Ru. (d) Powder X-ray diffraction patterns of simulated ZIF-8, ZIF-8, ZIF-8/Ru, and ZIF-8/Ru@TPE. (e) XPS spectra of ZIF-8, ZIF-8/Ru, and ZIF-8/Ru@TPE in the Ru 3p region. (f) Hydrodynamic diameters of ZIF-8/Ru and ZIF-8/Ru@TPE as measured by dynamic light scattering. Error bars represent the standard deviation of three independent measurements. (g) SEM image of ZIF-8/Ru@TPE.

the reaction medium, and 10 μg/mL of ZIF-8/Ru or ZIF-8/Ru@TPE nanozymes were used for kinetic measurements. During the assay, the nanozymes were mixed with varying concentrations of one substrate (either H_2O_2 or TMB) while keeping the other constant (0.2 mM for TMB and 50 mM for H_2O_2). The absorbance at 652 nm was immediately monitored, and the obtained "Absorbance versus Time" curves were used to calculate the initial reaction velocity (v). The kinetic parameters, including the Michaelis−Menten constant (K_m) and the maximum reaction velocity (v_{max}), were derived by fitting the data to the Michaelis−Menten equation as follows:

$$v = \frac{v_{max}[S]}{K_m + [S]} \quad (1)$$

where v represents the initial reaction velocity, [S] is the substrate concentration. K_m and v_{max} were calculated from the double reciprocal plots derived from the equation.

Ratiometric Detection of H_2O_2 and Glucose

For ratiometric detection of H_2O_2, 10 μg/mL ZIF-8/Ru@TPE and 5 mM *o*-phenylenediamine (OPD) were dispersed in 0.2 M acetate buffer (pH 4.5) containing various concentrations of H_2O_2 (0−20 mM). The reaction mixture was incubated at 26 °C for 40 min in the dark. Subsequently, 200 μL of the solution was transferred to a 96-well microplate, and the fluorescence emissions at 445 and 570 nm were recorded using a microplate reader with an excitation wavelength of 375 nm.

For glucose detection, 0.5 mg/mL glucose oxidase (GOx) and different concentrations of glucose were mixed in 20 mM Tris-HCl buffer (pH 7.5) and incubated at 37 °C for 40 min to generate H_2O_2 *in situ*. The resulting solution was then added to 0.2 M acetate buffer (pH 4.5) containing ZIF-8/Ru@TPE (10 μg/mL) and OPD (5 mM) and further incubated at 26 °C for 40 min in the dark. Finally, 200 μL of the reaction mixture was transferred to a 96-well microplate, and fluorescence intensities at 445 and 570 nm were measured upon excitation at 375 nm using a microplate reader.

AA Detection

ZIF-8/Ru@TPE (10 μg/mL) and OPD (5 mM) were mixed with varying concentrations of AA (0−2 mM) and 10 mM H_2O_2 in 0.2 M acetate buffer (pH 4.5). The reaction mixture was incubated at 26 °C for 40 min in the dark. Subsequently, 200 μL of the resulting solution was transferred to a 96-well microplate, and the fluorescence intensities were recorded using a microplate reader with an excitation wavelength of 375 nm and emission wavelengths of 445 and 570 nm. To evaluate the selectivity of the proposed assay toward AA, potential interfering substances, including 50 μM glutathione (GSH) and cysteine, were tested under identical conditions.

The AA contents of three vitamin C tablets and six commercial beverage samples were determined using the developed ratiometric fluorescence assay. The sample concentrations were first adjusted to fall within the linear detection range and subsequently analyzed following the same AA assay protocol.

https://doi.org/10.1021/acs.analchem.5c07377
Anal. Chem. XXXX, XXX, XXX−XXX

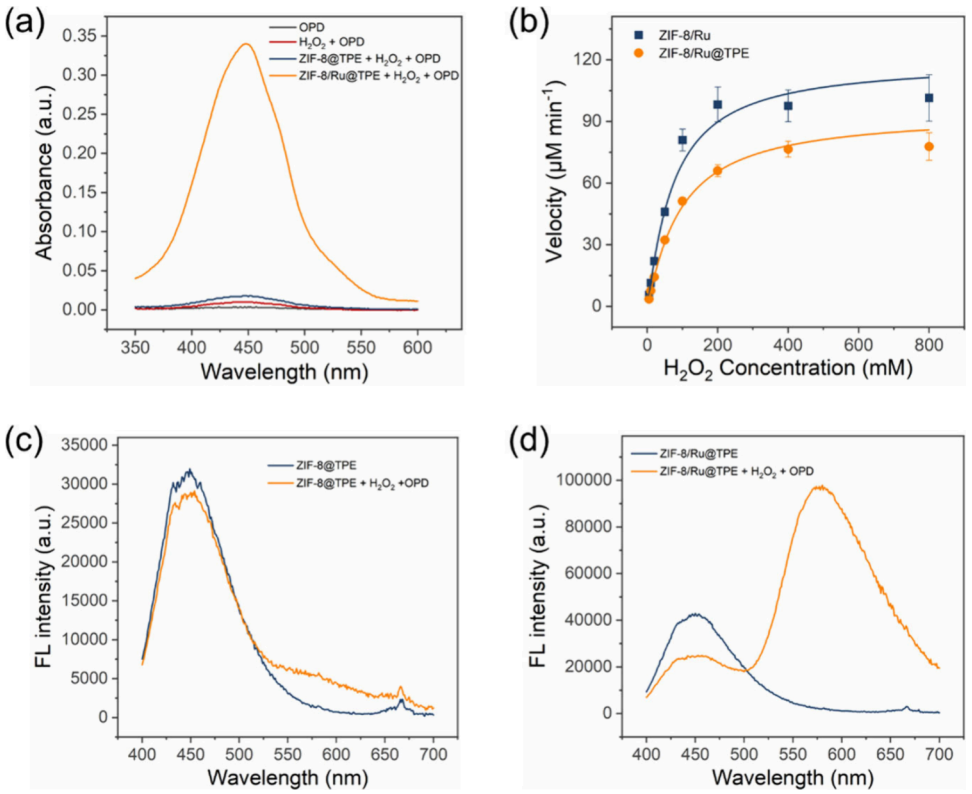

Figure 2. (a) UV−vis absorption spectra of different reaction systems after catalyzing oxidation in pH 4.5, 0.2 M acetate buffer for 5 min. (b) Plots of the initial reaction velocity versus H_2O_2 concentration in the presence of 0.2 mM TMB and 10 μg/mL of ZIF-8/Ru or ZIF-8/Ru@TPE in pH 4.5, 0.2 M acetate buffer. Error bars represent the standard deviation of three independent measurements. (c) Fluorescence spectra of ZIF-8@TPE and ZIF-8@TPE with H_2O_2 + OPD. (d) Fluorescence spectra of ZIF-8/Ru@TPE and ZIF-8/Ru@TPE with H_2O_2 + OPD.

ALP Activity Assay

For the ratiometric detection of ALP, 0.4 mM AAP and varying concentrations of ALP (0−200 U/L) were mixed in 20 mM Tris-HCl buffer (pH 8.5) and incubated at 37 °C for 40 min. After incubation, 0.2 M acetate buffer (pH 4.5) containing ZIF-8/Ru@TPE (10 μg/mL), OPD (5 mM), and H_2O_2 (10 mM) was sequentially added, and the mixture was further incubated at 26 °C for 40 min in the dark. Subsequently, 200 μL of the reaction solution was transferred into a 96-well microplate, and the fluorescence intensities were recorded using a microplate reader with an excitation wavelength of 375 nm and emission wavelengths at 445 and 570 nm.

For the detection of ALP activity in serum samples, 20 mM Tris-HCl buffer (pH 8.5) containing 0.4 mM AAP and 5% fetal bovine serum spiked with varying concentrations of ALP was incubated at 37 °C for 40 min. All subsequent procedures were performed as described above for the ALP assay.

RESULTS AND DISCUSSION

Synthesis and Characterization of ZIF-8/Ru@TPE

In this study, an aggregation-induced emission (AIE) fluorescent nanozyme, denoted as ZIF-8/Ru@TPE, was rationally designed for constructing a ratiometric biosensing platform (Figure 1a). Ultrasmall Ru nanoparticles with intrinsic peroxidase-like activity were synthesized via a hydrothermal method (Figure S1),[24] while ZIF-8 was prepared following previous procedures with modification to yield uniform polyhedral particles of ∼90 nm (Figure S2).[55] Ru nanoparticles were uniformly anchored onto ZIF-8 through a coprecipitation method to form ZIF-8/Ru, which exhibited a slightly larger average size (∼120 nm) compared with pristine ZIF-8 (Figures 1a, S2, and S3). TEM imaging confirmed the homogeneous distribution of Ru nanoparticles on the ZIF-8 surface, with a lattice spacing of 0.205 nm corresponding to the (101) plane of Ru (Figures 1b and S4). HAADF-STEM coupled with EDS elemental mappings further verified the uniform spatial distribution of Zn, C, and Ru elements throughout the composite (Figure 1c). ICP-OES analysis revealed that ZIF-8/Ru contained 7.1 wt % Ru (Table S1). The powder XRD pattern of ZIF-8/Ru remained consistent with that of pristine ZIF-8, indicating that the crystalline framework was well preserved after Ru incorporation (Figure 1d). No distinct diffraction peaks corresponding to Ru were observed, likely due to the ultrasmall particle size and low Ru content (Figures 1d, S1, and Table S1). XPS analysis further confirmed the successful incorporation of Ru, showing a characteristic Ru 3p signal at 461.5 eV (Figures 1e and S5), along with the C 1s, N 1s, O 1s, and Zn 2p peaks, confirming the successful synthesis of ZIF-8/Ru nanocomposites.

To impart dual catalytic and fluorescent functionalities, ZIF-8/Ru was further self-assembled with the AIE luminogen tetraphenylethylene (TPE) in aqueous solution, yielding the composite ZIF-8/Ru@TPE (Figure 1a; see the Experimental Section for details). XRD confirmed that the crystalline structure of ZIF-8 was preserved after the assembly process (Figure 1d). XPS spectra further verified the presence of Ru in ZIF-8/Ru@TPE, although the Ru signal intensity was slightly reduced compared with ZIF-8/Ru, which can be mainly attributed to the lower relative Ru content following TPE incorporation (Figure 1e and Table S1). Dynamic light scattering (DLS) measurements revealed a substantial increase in hydrodynamic diameter from 190.9 nm for ZIF-8/Ru to 1487.5 nm for ZIF-8/Ru@TPE (Figure 1f). SEM imaging

https://doi.org/10.1021/acs.analchem.5c07377
Anal. Chem. XXXX, XXX, XXX−XXX

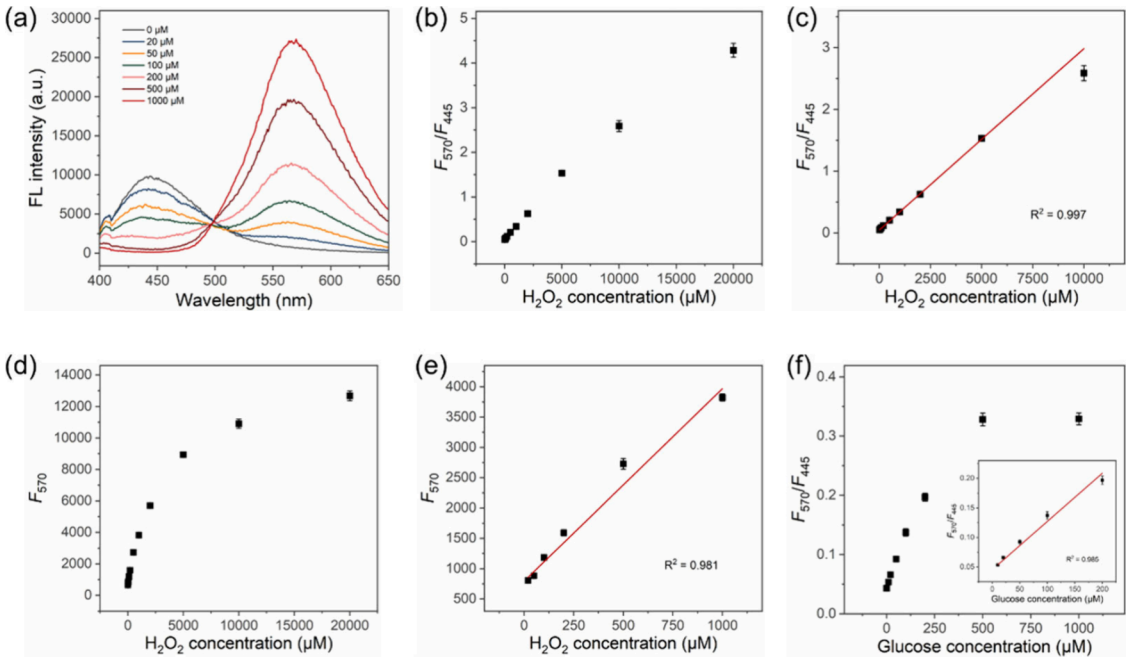

Figure 3. (a) Fluorescence spectra of ZIF-8/Ru@TPE in the presence of 5 mM OPD with varying H_2O_2 concentrations. (b) Fluorescence intensity ratio (F_{570}/F_{445}) as a function of H_2O_2 concentration. (c) Linear calibration curve of F_{570}/F_{445} versus H_2O_2 concentration (20−10000 μM). (d) Fluorescence intensity at 570 nm (F_{570}) as a function of H_2O_2 concentration. (e) Linear calibration curve of F_{570} versus H_2O_2 concentration (20−1000 μM). Error bars represent the standard deviation of four independent measurements. (f) Fluorescence intensity ratio (F_{570}/F_{445}) as a function of glucose concentration. Inset: corresponding linear calibration curve of F_{570}/F_{445} versus glucose concentration (10−200 μM). Error bars represent the standard deviation of three independent measurements.

directly visualized microscale TPE spheres decorated with ZIF-8/Ru nanoparticles, demonstrating the successful self-assembly (Figures 1g and S6). In addition, the comparable zeta potentials of ZIF-8/Ru and ZIF-8/Ru@TPE indicated that the ZIF-8/Ru particles were adsorbed onto the surfaces of the TPE microspheres rather than encapsulated within them (Figure S7). Collectively, these structural and compositional characterizations confirmed the successful synthesis of ZIF-8/Ru@TPE.

Peroxidase-like Activity and Fluorescent Property

After confirming the successful fabrication of ZIF-8/Ru@TPE, its catalytic and optical properties were systematically evaluated. To elucidate the effects of Ru nanoparticle incorporation and TPE assembly, ZIF-8@TPE was also synthesized under identical conditions and employed as a control (Figures S8 and S9). As shown in Figure 2a, the peroxidase-like activity of ZIF-8/Ru@TPE was first assessed through monitoring the oxidation of the chromogenic substrate *o*-phenylenediamine (OPD) in the presence of H_2O_2. A characteristic absorption peak centered at 450 nm appeared in the ZIF-8/Ru@TPE + OPD + H_2O_2 system, confirming its pronounced catalytic activity. In contrast, negligible absorption changes were observed for H_2O_2 and OPD alone or even in the presence of ZIF-8@TPE, indicating that ZIF-8@TPE exhibited minimal peroxidase-like activity. These findings demonstrated that the catalytic activity of ZIF-8/Ru@TPE originated from the Ru nanoparticles grown on the ZIF-8 surface. The catalytic performance of ZIF-8/Ru@TPE was further evaluated under various pH conditions, revealing strong pH dependence with the highest activity observed at pH 4.5 (Figure S10). To investigate the effect of TPE self-assembly on catalytic performance, steady-state kinetic assays were conducted to compare ZIF-8/Ru and ZIF-8/Ru@TPE with identical concentrations. As illustrated in Figures 2b and S11, typical Michaelis−Menten curves were obtained by plotting initial reaction rates against the concentrations of H_2O_2 or TMB. The corresponding kinetic parameters, including the Michaelis constant (K_m) and maximum reaction velocity (v_{max}), were derived from Lineweaver−Burk plots (Figures S12 and S13, and Table S2). Compared with ZIF-8/Ru, ZIF-8/Ru@TPE displayed slightly reduced peroxidase-like activity, with v_{max} values toward H_2O_2 determined to be 154.08 and 137.74 μM/min, respectively (Table S2). This decline in catalytic activity was mainly attributed to the reduced proportion of Ru nanoparticles in the overall ZIF-8/Ru@TPE composite after self-assembly, which led to fewer exposed active sites (Table S1).

The optical properties of ZIF-8/Ru@TPE were further explored to assess the fluorescence originating from the assembled TPE units. As shown in Figure S14, the UV−vis absorption spectrum of ZIF-8/Ru@TPE exhibited a distinct peak at 323 nm, corresponding to the characteristic of TPE absorption. To investigate whether ZIF-8/Ru@TPE retained the intrinsic optical behavior of TPE, fluorescence spectra were recorded and compared with those of reference materials (i.e., ZIF-8/Ru and ZIF-8@TPE). As shown in Figure S15, ZIF-8/Ru displayed negligible fluorescence but possessed distinct peroxidase-like catalytic activity, efficiently catalyzing the oxidation of OPD in the presence of H_2O_2 to generate the fluorescent product 2,3-diaminophenazine (DAP) with an emission at 570 nm. ZIF-8@TPE showed strong intrinsic emission peak at 445 nm upon excitation at 375 nm but exhibited no catalytic activity toward OPD oxidation (Figure 2c). Upon addition of H_2O_2 and OPD, only a weak fluorescence signal appeared at 570 nm, attributable to the slight self-oxidation of OPD (Figure 2c). In contrast, ZIF-8/

https://doi.org/10.1021/acs.analchem.5c07377
Anal. Chem. XXXX, XXX, XXX−XXX

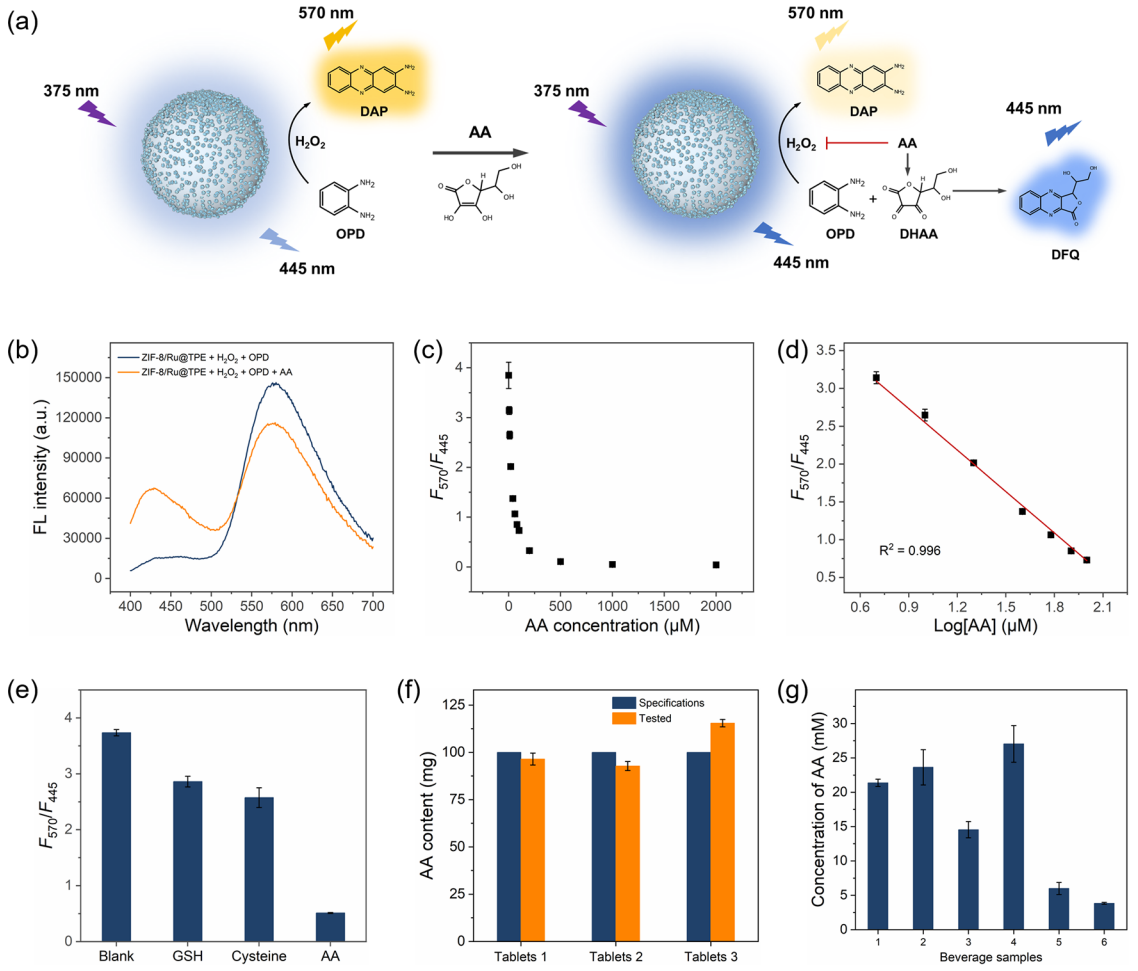

Figure 4. (a) Schematic illustration of a ratiometric sensing platform for AA detection. (b) Fluorescence spectra of ZIF-8/Ru@TPE reaction systems in the absence and presence of AA. (c) Fluorescence intensity ratio (F_{570}/F_{445}) as a function of AA concentration. (d) Linear calibration curve of F_{570}/F_{445} versus the logarithm of the AA concentration (5−100 μM). (e) Comparison of F_{570}/F_{445} responses to 50 μM GSH, cysteine, and AA. (f) Quantification of AA in three commercial vitamin tablets (labeled with specification values for comparison). (g) Quantification of AA in six commercial beverages (samples 1−6). Error bars represent the standard deviation of four independent measurements.

Ru@TPE exhibited dual-emission behavior, featuring a pronounced intrinsic emission at 445 nm and a reaction-induced emission at 570 nm upon the addition of H_2O_2 and OPD (Figure 2d). The catalytic oxidation of OPD by ZIF-8/Ru@TPE generated the fluorescent product DAP, resulting in the emergence of a distinct fluorescence peak at 570 nm, while the original TPE emission at 445 nm was partially quenched by DAP. These results clearly demonstrated that ZIF-8/Ru@TPE integrated both peroxidase-like activity and intrinsic fluorescences, originating from the Ru nanoparticles and TPE units, respectively. Furthermore, the fluorescence stability of ZIF-8/Ru@TPE was also examined. As shown in Figure S16, the emission intensity at 445 nm remained nearly unchanged after 40 min of incubation in aqueous solution, indicating excellent fluorescence stability. Moreover, sensing tests using three independently prepared dispersions produced highly consistent responses, confirming the good reproducibility of our method (Figure S17).

We also explored the direct assembly of Ru nanoparticles with TPE to form Ru@TPE. Although Ru could be deposited on the TPE microspheres and the resulting Ru@TPE retained both fluorescence and catalytic activity, TEM revealed a nonuniform Ru distribution with a fraction of unbound nanoparticles, which may lead to batch-to-batch variability and compromised sensing reproducibility (Figure S18).

Ratiometric Sensing of H_2O_2 and Glucose

Then, the fluorescent ZIF-8/Ru@TPE nanozyme, possessing intrinsic peroxidase-like activity, was employed to construct a ratiometric fluorescence sensing platform. ZIF-8/Ru@TPE was first applied for the detection of H_2O_2 and glucose. A schematic illustration of the sensing mechanism was shown in Figure S19. As revealed by fluorescence spectroscopy, ZIF-8/Ru@TPE exhibited a strong emission peak at 445 nm (Figure 3a). Upon the addition of H_2O_2 and OPD, OPD was catalytically oxidized by ZIF-8/Ru@TPE to produce DAP, which generated a new fluorescence emission at 570 nm. Meanwhile, due to the inner-filter effect (IFE) between DAP and ZIF-8/Ru@TPE,[40,51] the intrinsic emission of ZIF-8/Ru@TPE at 445 nm was gradually quenched. As shown in Figure 3a, increasing the H_2O_2 concentration led to a progressive enhancement of the fluorescence at 570 nm, accompanied by a simultaneous attenuation of the 445 nm emission. Consequently, the fluorescence intensity ratio (F_{570}/F_{445}) was adopted as a ratiometric signal output for the quantitative determination of H_2O_2. To assess the analytical performance of the system, the linear range and limit of detection (LOD) were

https://doi.org/10.1021/acs.analchem.5c07377
Anal. Chem. XXXX, XXX, XXX−XXX

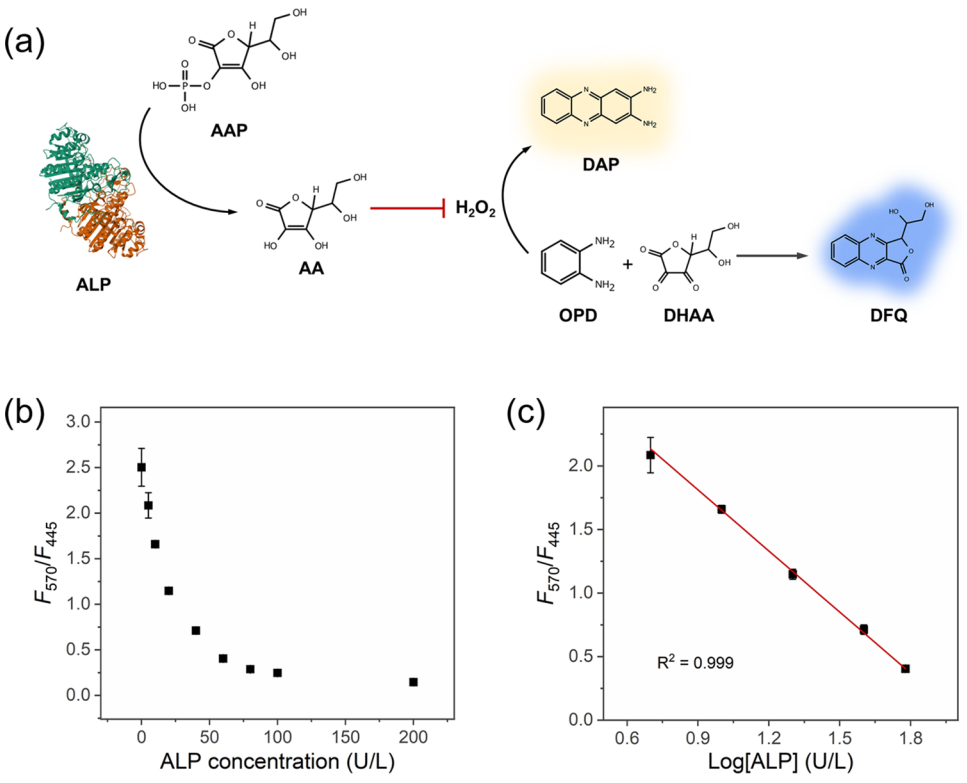

Figure 5. (a) Schematic illustration of the ZIF-8/Ru@TPE-based ratiometric sensing platform for ALP activity assay. (b) Fluorescence intensity ratio (F_{570}/F_{445}) as a function of ALP concentration. (c) Linear calibration curve of F_{570}/F_{445} versus the logarithm of ALP concentration (5−60 U/L). Error bars represent the standard deviation of four independent measurements.

evaluated by introducing various concentrations of H_2O_2 (20−20000 μM) into the ZIF-8/Ru@TPE and OPD reaction system, and the corresponding F_{570}/F_{445} were recorded (Figure 3b). The ratiometric sensing platform exhibited a wide linear response toward H_2O_2 in the range of 20−10000 μM, with a calculated LOD of 10.62 μM based on the F_{570}/F_{445} signal (Figure 3c). To further demonstrate the advantages of the ratiometric strategy, a conventional single-emission mode using the DAP fluorescence intensity at 570 nm (F_{570}) as the output signal was also examined. As shown in Figure 3d,e, F_{570} gradually increased with increasing H_2O_2 concentration, giving a narrower linear range of 20−1000 μM and a higher LOD of 28.40 μM. These results clearly highlighted that the ratiometric fluorescence sensing strategy offered superior analytical performance, featuring a broader dynamic range and enhanced sensitivity compared with single-signal detection approaches.

Encouraged by the above results, the ZIF-8/Ru@TPE-based ratiometric sensing platform was further extended to detect H_2O_2-generating metabolites. In this study, glucose was selected as a representative analyte to validate the applicability of the ratiometric sensing platform (Figure S19). As illustrated in Figure S19, glucose was specifically oxidized by glucose oxidase (GOx) to produce H_2O_2, which subsequently acted as the substrate for the ZIF-8/Ru@TPE-catalyzed oxidation of OPD, yielding the fluorescent product DAP for signal readout. As shown in Figure 3f, the fluorescence intensity ratio (F_{570}/F_{445}) gradually increased with increasing glucose concentration. The developed ratiometric fluorescence assay displayed an excellent linear response in the range of 10−200 μM, with a detection limit of 5.36 μM. These above findings confirmed the potential of ZIF-8/Ru@TPE for constructing ratiometric sensing platforms for advanced biosensing applications.

Selective Detection of AA Using a Ratiometric Sensing Platform

It has been previously reported that nonfluorescent *o*-phenylenediamine (OPD) could react with the oxidation product of ascorbic acid (AA), dehydroascorbic acid (DHAA), to form a fluorescent compound, 3-(1,2-dihydroxyethyl)furo-[3,4-*b*]quinoxalin-1(3H)-one (DFQ), exhibiting an emission peak around 445 nm.[39,56] As shown in Figure S20, AA was oxidized to dehydroascorbic acid (DHAA) through a Fenton reaction, and the resulting DHAA subsequently reacted with OPD to produce a distinct fluorescence emission at approximately 445 nm. Inspired by this mechanism, a self-amplified ratiometric fluorescence sensing strategy was developed using the ZIF-8/Ru@TPE nanozyme for the selective detection of AA (Figure 4a). In this system, AA inhibited the H_2O_2-driven catalytic oxidation of OPD to DAP, resulting in a decreased fluorescence intensity of DAP at 570 nm, accompanied by an enhanced intrinsic fluorescence signal of ZIF-8/Ru@TPE at 445 nm. Simultaneously, the produced DHAA reacts with residual OPD to generate DFQ, introducing a new fluorescence emission at 445 nm (Figure 4a). Consequently, with increasing AA concentration, the emission at 570 nm gradually decreased while that at 445 nm intensified, producing a distinct self-amplified ratiometric fluorescence response (Figure 4b). As shown in Figure 4c, the fluorescence intensity ratio (F_{570}/F_{445}) decreased exponentially with increasing AA concentration, in accordance with the proposed self-amplified mechanism. A calibration plot of F_{570}/F_{445} versus the logarithm of AA concentration exhibited a good linear relationship in the range of 5−100 μM, with a calculated detection limit of 2.71 μM (Figure 4d). These results demonstrated that the ZIF-8/Ru@TPE-based ratiometric

https://doi.org/10.1021/acs.analchem.5c07377
Anal. Chem. XXXX, XXX, XXX−XXX

sensing platform enabled sensitive and reliable detection of AA through fluorescence signal modulation.

To further evaluate the selectivity of the proposed ratiometric sensing platform, potential interfering antioxidants such as glutathione (GSH) and cysteine were tested under identical conditions. As shown in Figures 4e and S21, GSH and cysteine induced only minor variations in the F_{570}/F_{445} ratio, as they merely competed with the substrate in the peroxidase-like reaction without producing DFQ fluorescence at 445 nm. In contrast, AA elicited a distinct ratiometric response attributed to the self-amplified mechanism (Figures 4e and S21). Notably, when the assay was performed using a single-emission readout (F_{570}), both GSH and cysteine generated responses comparable to AA, underscoring the limited selectivity of conventional single-signal nanozyme assays, which was consistent with previous findings (Figure S22 and Table S3).[37−41]

Finally, the practical applicability of the proposed assay was verified by quantifying AA in commercial vitamin C tablets and beverages. As shown in Figure 4f, the measured AA concentrations in three types of vitamin C tablets were consistent with their labeled values, confirming the accuracy and reliability of the ratiometric sensing platform. Likewise, comparable results were obtained for six beverage samples, among which beverages 1, 2, and 4 contained higher AA levels than 3, 5, and 6 (Figure 4g). Collectively, these results demonstrated the strong potential of ZIF-8/Ru@TPE as a fluorescent nanozyme for constructing self-amplified ratiometric sensing platforms with reliable analytical performance and practical applicability.

Detemination of ALP Activity in Serum Samples

Alkaline phosphatase (ALP) is an essential enzyme broadly distributed in human tissues and body fluids. Abnormal ALP activity is closely linked to a variety of pathological conditions, including bone diseases, liver dysfunction, and prostate cancer. Hence, the development of a reliable analytical platform capable of sensitively and selectively detecting ALP activity holds great clinical significance. As illustrated in Figure 5a, ALP catalyzed the hydrolysis of AAP to generate ascorbic acid (AA), which subsequently triggered a self-amplified ratiometric fluorescence response within the ZIF-8/Ru@TPE reaction system. By coupling the ALP-catalyzed hydrolysis with the nanozyme-mediated sensing process, a ratiometric fluorescence platform was constructed for quantitative evaluation of ALP activity (Figure 5a). As shown in Figure 5b, the fluorescence intensity ratio (F_{570}/F_{445}) decreased progressively with increasing ALP concentration. A clear linear relationship between F_{570}/F_{445} and ALP concentration was established over the range of 5−60 U/L (Figure 5c), with a detection limit of 2.43 U/L.

To further evaluate the practical applicability of the developed assay, it was employed to determine ALP activity in serum samples. As summarized in Table 1, the recoveries of four spiked serum samples ranged from 90.35% to 129.25%, with relative standard deviations (RSDs) below 5.55%. The single-signal approach yielded substantially overestimated recoveries and larger RSDs compared with the ratiometric assay, likely due to interference from endogenous reducing species in serum (Figure S23 and Table S4). These results demonstrated that the ZIF-8/Ru@TPE-based ratiometric fluorescence platform offered high analytical reliability and strong potential for accurate determination of ALP activity in complex biological matrices.

Table 1. Results for the Determination of ALP in Serum Samples

Added (U/L)	Found (U/L)	Recovery (%)	RSD (n = 4)
8	10.34	129.25%	4.37%
10	12.32	123.20%	5.55%
16	16.20	101.25%	1.93%
20	18.07	90.35%	1.47%

CONCLUSIONS

In conclusion, ZIF-8/Ru@TPE was successfully constructed by assembling Ru nanoparticle-decorated ZIF-8 with TPE luminogen. ZIF-8/Ru@TPE integrated intrinsic fluorescence and peroxidase-like catalytic activity, enabling the establishment of a ratiometric fluorescence platform for quantitative detection of H_2O_2 and glucose with wide linear ranges and low detection limits. Based on the specific reaction between dehydroascorbic acid and OPD, a self-amplified ratiometric fluorescence assay was further developed for highly selective ascorbic acid detection over other reductants. Furthermore, by coupling with alkaline phosphatase-catalyzed hydrolysis of AAP, the system allowed accurate determination of ALP activity in serum samples. In future work, the relative content and spatial distribution of TPE and Ru will be optimized to better balance the dual-emission signals and further improve ratiometric sensing performance. Overall, this study presents a versatile nanozyme-based strategy for constructing selective ratiometric sensing platforms and provides new insights into the rational design of multifunctional catalytic materials for bioanalytical applications.

ASSOCIATED CONTENT

Supporting Information

The Supporting Information is available free of charge at https://pubs.acs.org/doi/10.1021/acs.analchem.5c07377.

TEM images of ZIF-8/Ru; SEM images and XPS survey scans of ZIF-8/Ru@TPE; zeta potentials of ZIF-8/Ru and ZIF-8/Ru@TPE; fluorescence intensity ratio (F_{570}/F_{445}) changes using three independently prepared ZIF-8/Ru@TPE dispersions; fluorescence spectra of ZIF-8/Ru@TPE reaction systems in the absence and presence of GSH, cysteine, and AA; comparison of kinetic parameters of ZIF-8/Ru and ZIF-8/Ru@TPE; results for the determination of ALP in serum samples using the single-signal method (PDF)

AUTHOR INFORMATION

Corresponding Authors

Xiaoyu Wang − *Department of Chemistry and Material Science, College of Science, Nanjing Forestry University, Nanjing, Jiangsu 210037, China; College of Engineering and Applied Sciences, Nanjing National Laboratory of Microstructures, Jiangsu Key Laboratory of Artificial Functional Materials, Nanjing University, Nanjing, Jiangsu 210023, China*; Email: wangxiaoyu@njfu.edu.cn

Hui Wei − *College of Engineering and Applied Sciences, Nanjing National Laboratory of Microstructures, Jiangsu Key Laboratory of Artificial Functional Materials and State Key Laboratory of Analytical Chemistry for Life Science, School of*

https://doi.org/10.1021/acs.analchem.5c07377
Anal. Chem. XXXX, XXX, XXX−XXX

Chemistry and Chemical Engineering, Chemistry and Biomedicine Innovation Center (ChemBIC), ChemBioMed Interdisciplinary Research Center at Nanjing University, Nanjing University, Nanjing, Jiangsu 210023, China; NMPA Key Laboratory for Biomedical Optics, Hangzhou, Zhejiang 310018, China; orcid.org/0000-0003-0870-7142; Email: weihui@nju.edu.cn

Authors

Sijie Li − *Department of Chemistry and Material Science, College of Science, Nanjing Forestry University, Nanjing, Jiangsu 210037, China*

Si Zhang − *Key Laboratory of Quantum Materials and Devices of Ministry of Education, School of Physics, Southeast University, Nanjing 211189, China*

Qi Sun − *College of Engineering and Applied Sciences, Nanjing National Laboratory of Microstructures, Jiangsu Key Laboratory of Artificial Functional Materials, Nanjing University, Nanjing, Jiangsu 210023, China;* orcid.org/0009-0004-3613-2774

Qing Cheng − *Department of Chemistry and Material Science, College of Science, Nanjing Forestry University, Nanjing, Jiangsu 210037, China*

Ke Bao − *Department of Chemistry and Material Science, College of Science, Nanjing Forestry University, Nanjing, Jiangsu 210037, China*

Bing Xia − *Department of Chemistry and Material Science, College of Science, Nanjing Forestry University, Nanjing, Jiangsu 210037, China;* orcid.org/0000-0002-1637-7908

Complete contact information is available at: https://pubs.acs.org/10.1021/acs.analchem.5c07377

Author Contributions

All authors have given approval to the final version of the manuscript.

Notes

The authors declare no competing financial interest.

■ ACKNOWLEDGMENTS

This work was supported by the Natural Science Foundation of Jiangsu Province (BK20241895), Jiangsu Provincial Key R&D Program (BE2022836), the National Natural Science Foundation of China (22104055, 22374071, and 22477060), the State Key Laboratory of Analytical Chemistry for Life Science (5431ZZXM2501), the Fundamental Research Funds for the Central Universities (2025300292), the PAPD Program, the Key Program of Nanozyme Laboratory in Zhongyuan (NLZ-KP2024NIC06), Open Funds of NMPA Key Laboratory for Biomedical Optics (20240001), and the International Expansion and Enhancement Program by Nanjing University International Affairs Office.

■ REFERENCES

(1) Gao, L.; Zhuang, J.; Nie, L.; Zhang, J.; Zhang, Y.; Gu, N.; Wang, T.; Feng, J.; Yang, D.; Perrett, S.; et al. Intrinsic peroxidase-like activity of ferromagnetic nanoparticles. *Nat. Nanotechnol.* **2007**, *2* (9), 577−583.

(2) Wu, J.; Wang, X.; Wang, Q.; Lou, Z.; Li, S.; Zhu, Y.; Qin, L.; Wei, H. Nanomaterials with enzyme-like characteristics (nanozymes): next-generation artificial enzymes (II). *Chem. Soc. Rev.* **2019**, *48* (4), 1004−1076.

(3) Huang, Y.; Ren, J.; Qu, X. Nanozymes: classification, catalytic mechanisms, activity regulation, and applications. *Chem. Rev.* **2019**, *119* (6), 4357−4412.

(4) Zandieh, M.; Liu, J. W. Nanozymes: Definition, Activity, and Mechanisms. *Adv. Mater.* **2024**, *36* (10), No. 2211041.

(5) Wei, H.; Gao, L.; Fan, K.; Liu, J.; He, J.; Qu, X.; Dong, S.; Wang, E.; Yan, X. Nanozymes: A clear definition with fuzzy edges. *Nano Today* **2021**, *40*, No. 101269.

(6) Dong, H.; Du, W.; Dong, J.; Che, R.; Kong, F.; Cheng, W.; Ma, M.; Gu, N.; Zhang, Y. Depletable peroxidase-like activity of Fe_3O_4 nanozymes accompanied with separate migration of electrons and iron ions. *Nat. Commun.* **2022**, *13*, 5365.

(7) Zhang, Y.; Wei, G.; Liu, W.; Li, T.; Wang, Y.; Zhou, M.; Liu, Y.; Wang, X.; Wei, H. Nanozymes for nanohealthcare. *Nat. Rev. Methods Primers* **2024**, *4*, 36.

(8) Zhang, R.; Jiang, B.; Fan, K.; Gao, L.; Yan, X. Designing nanozymes for in vivo applications. *Nat. Rev. Bioeng.* **2024**, *2*, 849−868.

(9) Zhang, R. F.; Yan, X. Y.; Gao, L. Z.; Fan, K. L. Nanozymes expanding the boundaries of biocatalysis. *Nat. Commun.* **2025**, *16*, 6817.

(10) Liu, J.; Wang, M. J.; Yang, X.; Chen, H. Y.; Wei, M. J.; Zhu, X. H.; Zhang, Y. Y.; Liu, M. L.; Yao, S. Z. Covalent conjugation of doxorubicin to polydopamine on the surface of single-atom nanozyme for effective synergistic cancer therapy. *Sci. China Chem.* **2025**, *68* (8), 3852−3867.

(11) Shamsabadi, A.; Haghighi, T.; Carvalho, S.; Frenette, L. C.; Stevens, M. M. The Nanozyme Revolution: Enhancing the Performance of Medical Biosensing Platforms. *Adv. Mater.* **2024**, *36* (10), No. 2300184.

(12) Li, S.; Zhang, Y.; Wang, Q.; Lin, A.; Wei, H. Nanozyme-Enabled Analytical Chemistry. *Anal. Chem.* **2022**, *94* (1), 312−323.

(13) Jin, H.; Ye, D. X.; Shen, L. H.; Fu, R. X.; Tang, Y.; Jung, J. C. Y.; Zhao, H. B.; Zhang, J. J. Perspective for Single Atom Nanozymes Based Sensors: Advanced Materials, Sensing Mechanism, Selectivity Regulation, and Applications. *Anal. Chem.* **2022**, *94* (3), 1499−1509.

(14) Li, R.; Jiao, L.; Jia, X.; Yan, L.; Li, X.; Yan, D.; Zhai, Y.; Zhu, C.; Lu, X. Bioinspired FeN_5 Sites with Enhanced Peroxidase-like Activity Enable Colorimetric Sensing of Uranyl Ions in Seawater. *Anal. Chem.* **2024**, *96* (7), 3124−3130.

(15) Dissanayake, M.; Somerville, S. V.; Soda, Y.; Yao, Y.; Duong, H. T. K.; Tilley, R. D.; Gooding, J. J. An Array of Glucose Nanozymes That Can Selectively Detect Glucose in Whole Blood. *ACS Sens.* **2025**, *10* (1), 545−552.

(16) Liu, Y. F.; Zhang, J.; Wan, Y. X.; Li, C.; Cui, S.; Gao, X. J.; Wei, H.; Yang, D. Z. Engineering Perovskite Hydroxide as a Cold-Adapted Oxidase Mimic for Construction of the Robust Low-Temperature Adaptive Biosensors. *ACS Sens.* **2025**, *10* (3), 1844−1856.

(17) Guo, J. Y.; Wang, G.; She, Y. F.; Li, K.; Liu, Y. J.; Sun, Z. Y.; Chen, Z. B. Atomic Engineering of a FeFe Dual Single-Atom Nanozyme for Enhanced Peroxidase-like Activities To Build Chemical Tongue for Discrimination of Aromatic Amines. *Anal. Chem.* **2025**, *97* (36), 19889−19899.

(18) Qin, Y.; Liang, H. M.; Wu, J.; Chi, Z. Y.; Zhao, S. L.; Ye, F. G. Self-Cascade of the Cu/Ce-MOF-808 Nanozyme for One-Step Colorimetric Sensing. *Anal. Chem.* **2025**, *97* (15), 8468−8475.

(19) Yu, Z.; Xu, Z.; Zeng, R.; Xu, M.; Zheng, H.; Huang, D.; Weng, Z.; Tang, D. D-Band-Center-Engineered Platinum-Based Nanozyme for Personalized Pharmacovigilance. *Angew. Chem., Int. Ed.* **2025**, *64* (2), No. e202414625.

(20) He, R. W.; Guo, L. H.; Kou, X. X.; Gao, R.; Huang, W.; Zhong, N. Y.; Li, Z. W.; Huang, S. Y.; Huang, S. M.; Chen, G. S.; et al. Hierarchically Macroporous Ce-MOF Nanozyme with Enhanced Phosphoester Hydrolase- and Oxidase-like Activities for Self-Cascade Colorimetric Detection of Profenofos On-Site. *Anal. Chem.* **2025**, *97* (21), 11221−11230.

(21) Zhang, X. Z.; Lin, S. C.; Huang, R.; Gupta, A.; Fedeli, S.; Cao-Milan, R.; Luther, D. C.; Liu, Y. C.; Jiang, M. D.; Li, G. T.; et al. Degradable ZnS-Supported Bioorthogonal Nanozymes with En-

hanced Catalytic Activity for Intracellular Activation of Therapeutics. *J. Am. Chem. Soc.* **2022**, *144* (28), 12893−12900.
(22) Broto, M.; Kaminski, M. M.; Adrianus, C.; Kim, N.; Greensmith, R.; Dissanayake-Perera, S.; Schubert, A. J.; Tan, X.; Kim, H.; Dighe, A. S.; et al. Nanozyme-catalysed CRISPR assay for preamplification-free detection of non-coding RNAs. *Nat. Nanotechnol.* **2022**, *17* (10), 1120−1126.
(23) Qian, X. M.; Westensee, I. N.; Fernandes, C. C.; Städler, B. Enzyme Mimic Facilitated Artificial Cell to Mammalian Cell Signal Transfer. *Angew. Chem., Int. Ed.* **2021**, *60* (34), 18704−18711.
(24) Wang, X. Y.; Qin, L.; Zhou, M.; Lou, Z. P.; Wei, H. Nanozyme Sensor Arrays for Detecting Versatile Analytes from Small Molecules to Proteins and Cells. *Anal. Chem.* **2018**, *90* (19), 11696−11702.
(25) Guo, X. Y.; Wu, L. L.; Ma, L. Z.; Han, L. White Nanozymes with Enhanced Alkaline Phosphatase-Mimicking Activity and Selective Inhibition Effect: Enzyme-Free Colorimetric Test Strip of Pesticide. *Adv. Funct. Mater.* **2026**, *36*, No. e09324.
(26) Chai, L.; Chen, H. Y.; Yang, X.; Liu, J.; Yang, Q. Q.; Huang, S.; Tang, M.; Zhu, X. H.; Li, H. T.; Zhang, Y. Y.; et al. MnO_2 nanozyme-based ratiometric fluorescent nanoplatform for glutathione detection and intracellular imaging. *Talanta* **2026**, *297*, No. 128645.
(27) Fan, H. Z.; Zhang, R. F.; Fan, K. L.; Gao, L. Z.; Yan, X. Y. Exploring the Specificity of Nanozymes. *ACS Nano* **2024**, *18* (4), 2533−2540.
(28) Wei, G.; Liu, S. J.; Peng, Y. K.; Wei, H. On the Specificity of Nanozymes: A Perspective. *Chin. J. Chem.* **2024**, *42* (13), 1515−1522.
(29) Somerville, S. V.; Li, Q. Y.; Wordsworth, J.; Jamali, S.; Eskandarian, M. R.; Tilley, R. D.; Gooding, J. J. Approaches to Improving the Selectivity of Nanozymes. *Adv. Mater.* **2024**, *36* (10), No. 2211288.
(30) Park, S.; Shim, K. I.; Nguyen, P. T.; Choi, D.; Kim, S.; Yi, S. Y.; Kim, M. I.; Han, J. W.; Lee, J. Breaking the Selectivity Barrier of Single-Atom Nanozymes Through Out-of-Plane Ligand Coordination. *Adv. Mater.* **2025**, *37* (38), No. 2506480.
(31) Zhang, Z. J.; Zhang, X. H.; Liu, B. W.; Liu, J. W. Molecular Imprinting on Inorganic Nanozymes for Hundred-fold Enzyme Specificity. *J. Am. Chem. Soc.* **2017**, *139* (15), 5412−5419.
(32) O'Mara, P. B.; Wilde, P.; Benedetti, T. M.; Andronescu, C.; Cheong, S.; Gooding, J. J.; Tilley, R. D.; Schuhmann, W. Cascade Reactions in Nanozymes: Spatially Separated Active Sites inside Ag-Core-Porous-Cu-Shell Nanoparticles for Multistep Carbon Dioxide Reduction to Higher Organic Molecules. *J. Am. Chem. Soc.* **2019**, *141* (36), 14093−14097.
(33) Hong, Q.; Yang, H.; Fang, Y.; Li, W.; Zhu, C.; Wang, Z.; Liang, S.; Cao, X.; Zhou, Z.; Shen, Y.; et al. Adaptable graphitic C_6N_6-based copper single-atom catalyst for intelligent biosensing. *Nat. Commun.* **2023**, *14*, 2780.
(34) Xi, Z.; Wei, K.; Wang, Q.; Kim, M. J.; Sun, S.; Fung, V.; Xia, X. Nickel-Platinum Nanoparticles as Peroxidase Mimics with a Record High Catalytic Efficiency. *J. Am. Chem. Soc.* **2021**, *143* (7), 2660−2664.
(35) Hu, W.-C.; Pang, J.; Biswas, S.; Wang, K.; Wang, C.; Xia, X.-H. Ultrasensitive Detection of Bacteria Using a 2D MOF Nanozyme-Amplified Electrochemical Detector. *Anal. Chem.* **2021**, *93* (24), 8544−8552.
(36) Smirnoff, N. Ascorbic acid metabolism and functions: A comparison of plants and mammals. *Free Radic. Biol. Med.* **2018**, *122*, 116−129.
(37) Lou, Z.; Zhao, S.; Wang, Q.; Wei, H. N-Doped Carbon As Peroxidase-Like Nanozymes for Total Antioxidant Capacity Assay. *Anal. Chem.* **2019**, *91* (23), 15267−15274.
(38) Jiang, X. Q.; Wang, X. Y.; Lin, A. Q.; Wei, H. In Situ Exsolution of Noble-Metal Nanoparticles on Perovskites as Enhanced Peroxidase Mimics for Bioanalysis. *Anal. Chem.* **2021**, *93* (14), 5954−5962.
(39) Tao, C. Y.; Jiang, Y. Y.; Chu, S. S.; Miao, Y. R.; Zhang, J. Q.; Lu, Y. Z.; Niu, L. Natural Enzyme-Inspired Design of the Single-Atom Cu Nanozyme as Dual-Enzyme Mimics for Distinguishing Total Antioxidant Capacity and the Ascorbic Acid Level. *Anal. Chem.* **2024**, *96* (7), 3107−3115.
(40) Wu, S.; Yu, Z.; Zhao, J.; Wang, Y.; Nan, J.; Xu, L.; Li, X.; Yang, L.; Dong, S. Fluorescent Nanozyme Based on Bimetallic Fe/Co-Doped Carbon Dots for Dual-Mode Detection of Ascorbic Acid and Hydrogen Peroxide. *Anal. Chem.* **2025**, *97* (28), 15320−15328.
(41) Chen, Y. F.; Jiao, L.; Yan, H. Y.; Xu, W. Q.; Wu, Y.; Wang, H. J.; Gu, W. L.; Zhu, C. Z. Hierarchically Porous S/N Codoped Carbon Nanozymes with Enhanced Peroxidase-like Activity for Total Antioxidant Capacity Biosensing. *Anal. Chem.* **2020**, *92* (19), 13518−13524.
(42) Shen, X. Y.; Ma, S. R.; Song, C. C.; He, Y. Z.; Li, M. G. Kinetic and Mechanistic Discrepancies of Single/Dual-Atom Nanozymes Drive a Triple-Channel Sensing Array for Machine Learning-Assisted Antioxidant Discrimination. *Anal. Chem.* **2025**, *97* (36), 19957−19970.
(43) Wang, X. Y.; Wei, G.; Liu, W. L.; Zhang, Y. H.; Zhu, C. X.; Sun, Q.; Zhang, M. X.; Wei, H. Platinum-Nickel Nanoparticles with Enhanced Oxidase-like Activity for Total Antioxidant Capacity Bioassay. *Anal. Chem.* **2023**, *95* (14), 5937−5945.
(44) Li, X.; Yang, X. Q.; Wu, J.; Yang, Z. J.; Zhu, X. S. A Novel Four-Channel Sensor Array with Dual Enzymes and Dual Modes for Evaluating Total Antioxidant Capacity in Foods. *ACS Sens.* **2025**, *10* (4), 2883−2894.
(45) Kaliannan, K.; Hamarneh, S. R.; Economopoulos, K. P.; Alam, S. N.; Moaven, O.; Patel, P.; Malo, N. S.; Ray, M.; Abtahi, S. M.; Muhammad, N.; et al. Intestinal alkaline phosphatase prevents metabolic syndrome in mice. *Proc. Natl. Acad. Sci. U. S. A.* **2013**, *110* (17), 7003−7008.
(46) Lee, J.; Bubar, C. T.; Moon, H. G.; Kim, J.; Busnaina, A.; Lee, H.; Shefelbine, S. J. Measuring Bone Biomarker Alkaline Phosphatase with Wafer-Scale Nanowell Array Electrodes. *ACS Sens.* **2018**, *3* (12), 2709−2715.
(47) Song, Y.; Huang, C.; Li, Y. Nanozyme Rich in Oxygen Vacancies Derived from Mn-Based Metal-Organic Gel for the Determination of Alkaline Phosphatase. *Inorg. Chem.* **2023**, *62* (32), 12697−12707.
(48) Liu, W. D.; Chu, L.; Zhang, C. H.; Ni, P. J.; Jiang, Y. Y.; Wang, B.; Lu, Y. Z.; Chen, C. X. Hemin-assisted synthesis of peroxidase-like Fe-N-C nanozymes for detection of ascorbic acid-generating bio-enzymes. *Chem. Eng. J.* **2021**, *415*, No. 128876.
(49) Wang, X. Y.; Qin, L.; Lin, M. J.; Xing, H.; Wei, H. Fluorescent Graphitic Carbon Nitride-Based Nanozymes with Peroxidase-Like Activities for Ratiometric Biosensing. *Anal. Chem.* **2019**, *91* (16), 10648−10656.
(50) Teng, L.; Han, X.; Liu, Y.; Lu, C.; Yin, B.; Huan, S.; Yin, X.; Zhang, X.-B.; Song, G. Smart Nanozyme Platform with Activity-Correlated Ratiometric Molecular Imaging for Predicting Therapeutic Effects. *Angew. Chem., Int. Ed.* **2021**, *60* (50), 26142−26150.
(51) Shen, Y.; Wei, Y.; Gao, X.; Nie, C.; Wang, J.; Wu, Y. Engineering an Enzymatic Cascade Catalytic Smartphone-Based Sensor for Onsite Visual Ratiometric Fluorescence-Colorimetric Dual-Mode Detection of Methyl Mercaptan. *Environ. Sci. Technol.* **2023**, *57* (4), 1680−1691.
(52) Zhou, X. M.; Huang, S. J.; Guo, W. F.; Liu, W. F.; Wen, M. Y.; Shang, L. Multicolor Gold Clusterzyme-Enabled Construction of Ratiometric Fluorescent Sensor Array for Visual Biosensing. *Anal. Chem.* **2024**, *96* (47), 18873−18879.
(53) Jiang, B.; Duan, D.; Gao, L.; Zhou, M.; Fan, K.; Tang, Y.; Xi, J.; Bi, Y.; Tong, Z.; Gao, G. F.; et al. Standardized assays for determining the catalytic activity and kinetics of peroxidase-like nanozymes. *Nat. Protoc.* **2018**, *13* (7), 1506−1520.
(54) Zheng, J. J.; Zhu, F. Y.; Song, N. N.; Deng, F.; Chen, Q.; Chen, C.; He, J. Y.; Gao, X. F.; Liang, M. M. Optimizing the standardized assays for determining the catalytic activity and kinetics of peroxidase-like nanozymes. *Nat. Protoc.* **2024**, *19* (12), 3470−3488.
(55) Mu, J.; Li, C. X.; Shi, Y.; Liu, G. Y.; Zou, J. H.; Zhang, D. Y.; Jiang, C.; Wang, X. L.; He, L. C.; Huang, P.; et al. Protective effect of platinum nano-antioxidant and nitric oxide against hepatic ischemia-reperfusion injury. *Nat. Commun.* **2022**, *13*, 2513.

https://doi.org/10.1021/acs.analchem.5c07377
Anal. Chem. XXXX, XXX, XXX−XXX

(56) Luo, M. Y.; Zhang, K. H.; Rao, H. H.; Li, J. Y.; Xue, X.; Sun, P. P.; Lu, X. Q.; Xue, Z. H. A simplified ratiometric fluorescent sensing strategy for enhanced detection of alkaline phosphatase employing Prussian blue nanozymes and commercially available chromogen. *Chin. Chem. Lett.* **2025**, *36* (9), No. 110703.

https://doi.org/10.1021/acs.analchem.5c07377
Anal. Chem. XXXX, XXX, XXX−XXX